HHS Public Access

Author manuscript

*Mol Cell Neurosci*. Author manuscript; available in PMC 2023 July 10.

Published in final edited form as:

*Mol Cell Neurosci*. 2021 June ; 113: 103615. doi:10.1016/j.mcn.2021.103615.

# Kv1.1 subunits localize to cardiorespiratory brain networks in mice where their absence induces astrogliosis and microgliosis

**Hemangini A Dhaibar**[a], **Kathryn A Hamilton**[a], **Edward Glasscock**[a,b,*]

[a]Department of Cellular Biology & Anatomy, Louisiana State University Health Sciences Center, Shreveport, LA USA

[b]Department of Biological Sciences, Southern Methodist University, Dallas, TX USA

## Abstract

Cardiorespiratory collapse following a seizure is a suspected cause of sudden unexpected death in epilepsy (SUDEP), the leading cause of epilepsy-related mortality. In the commonly used *Kcna1* gene knockout (*Kcna1*$^{-/-}$) mouse model of SUDEP, cardiorespiratory profiling reveals an array of aberrant breathing patterns that could contribute to risk of seizure-related mortality. However, the brain structures mediating these respiratory abnormalities remain unknown. We hypothesize that Kv1.1 deficiency in respiratory control centers of the brain contribute to respiratory dysfunction in *Kcna1*$^{-/-}$ mice leading to increased SUDEP risk. Thus, in this study, we first used immunohistochemistry to map expression of Kv1.1 protein in cardiorespiratory brain regions of wild-type *Kcna1*$^{+/+}$ (WT) mice. Next, GFAP and Iba1 immunostaining was used to test for the presence of astrogliosis and microgliosis, respectively, in the cardiorespiratory centers of *Kcna1*$^{-/-}$ mice, which could be indicative of seizure-related brain injury that could impair breathing. In WT type mice, we detected Kv1.1 protein in all cardiorespiratory centers examined, including the basolateral amygdala, dorsal respiratory group, dorsal motor nucleus of vagus, nucleus ambiguus, ventral respiratory column, and pontine respiratory group, as well as chemosensory centers including the retrotrapezoid and median raphae nuclei. Extensive gliosis was observed in the same areas in *Kcna1*$^{-/-}$ mice suggesting that seizure-associated brain injury could contribute to respiratory abnormalities.

* **Corresponding author:** Edward Glasscock, Department of Biological Sciences, Southern Methodist University, Dallas, TX, 214-768-4050, eglasscock@smu.edu.

AUTHOR CONTRIBUTIONS

HD and EG conceived and designed the study and wrote the manuscript. HD performed the experiments and analyzed the data. KAH assisted with image acquisition, data analysis and interpretation, and manuscript editing.

CONFLICT OF INTEREST

None

**Ethics statement:** All experiments were performed in accordance with National Institutes of Health (NIH) guidelines with approval from the Institutional Animal Care and Use Committee of the Louisiana State University Health Sciences Center-Shreveport.

## 1. INTRODUCTION

Cardiorespiratory dysfunction is suspected as a primary risk factor for sudden unexpected death in epilepsy (SUDEP), the leading cause of epilepsy-related mortality, which is generally defined as the sudden death of someone with epilepsy for unknown reasons even following autopsy (Kennedy and Seyal 2015). Clinical studies of mortality in epilepsy monitoring units suggest that patients who succumb to SUDEP show a lethal cascade of seizure followed by terminal apnea, which appears to induce cardiac arrest (Ryvlin *et al.* 2013). Several mouse models also exhibit seizure-related respiratory arrest associated with increased risk of death, including the *Kcna1* gene knockout ($Kcna1^{-/-}$) mouse which is commonly used to study pathomechanisms underlying SUDEP (Feng and Faingold 2017; Kim *et al.* 2018; Kruse *et al.* 2019; Glasscock *et al.* 2010; Dhaibar *et al.* 2019; Wenker *et al.* 2021). $Kcna1^{-/-}$ mice lack Kv1.1 voltage-gated α-subunits, which control action potential firing properties in brain and heart, leading to spontaneous seizures that culminate in sudden premature death with onset at about two weeks old (Smart *et al.* 1998; Glasscock 2019). Cardiorespiratory profiling reveals primary breathing dysfunction during seizures in $Kcna1^{-/-}$ mice, including a high incidence of hyperventilation, tachypnea, and ataxic breathing, as well as occasional hypopnea, bradypnea, and apnea (Dhaibar *et al.* 2019). In addition, $Kcna1^{-/-}$ mice also exhibit basal breathing irregularities, including mild tachypnea, an absence of post-sigh apneas, a 3-fold increase in respiratory variability, and frequent hypoxia, which suggest Kv1.1 subunits play a fundamental role in regulating normal respiratory physiology (Dhaibar *et al.* 2019; Simeone *et al.* 2018).

The pathways and mechanisms contributing to breathing dysfunction in $Kcna1^{-/-}$ mice have not been identified in detail. Neuron–specific ablation of Kv1.1 in the central nervous system recapitulates most of the respiratory phenotypes seen in $Kcna1^{-/-}$ mice demonstrating a neural basis for the breathing abnormalities (Trosclair et al. 2020). In addition, Kv1.1 transcripts and protein are not detectable in the lungs of wild-type (WT) mice (Simeone *et al.* 2018). Kv1.1 exhibits widespread and primarily axonal expression in forebrain and cerebellar regions, but its localization in brainstem nuclei that control respiration has not been well characterized (Wang *et al.* 1994). In addition to the absence of Kv1.1 subunits in neurons that normally express them, Kv1.1 deficiency could also indirectly impair neural function by causing seizures which induce brain damage. One of the most common brain pathologies associated with epilepsy is reactive gliosis, a process whereby astrocytes and microglia become activated in response to injury and undergo morphological changes and increased proliferation that can promote neuronal hyperexcitability (Patel *et al.* 2019; Devinsky *et al.* 2013). In $Kcna1^{-/-}$ mice, seizures induce significant gliosis in the hippocampal formation and the hypothalamus, but other areas have not been investigated in detail (Wenzel *et al.* 2007; Roundtree *et al.* 2016).

Therefore, the goal of this work was to investigate the localization of Kv1.1 subunits in cardiorespiratory brain regions of WT mice and to determine whether the absence of Kv1.1 in $Kcna1^{-/-}$ mice leads to seizure–associated pathology in these neuronal populations that could potentially impair function. First, immunohistochemistry was used to map Kv1.1 protein localization in WT mice in the major brainstem nuclei that are responsible for the control of respiration and cardiac function. To identify seizure-related damage in

cardiorespiratory centers, astrogliosis and microgliosis were then assessed in *Kcna1*$^{-/-}$ brains by imaging immunoreactivity for glial fibrillary acidic (GFAP) protein and for ionized calcium binding adaptor molecule 1 (Iba1) protein, respectively. Our findings reveal prominent Kv1.1 immunoreactivity in respiratory brainstem regions where the channels could influence breathing intrinsically, as well as extensive gliosis in respiratory nuclei in *Kcna1*$^{-/-}$ mice suggesting the potential for impaired breathing due to seizure-induced injury.

## 2. MATERIALS AND METHODS

### 2.1 Animals and genotyping

*Kcna1*$^{-/-}$ mice (Tac:N:NIHS–BC genetic background) carry null knockout (KO) alleles of the *Kcna1* gene generated by targeted deletion of the entire open reading frame on chromosome 6 (Smart *et al.* 1998). Mice were housed at 22°C, fed ad libitum, and submitted to a 12-h light/dark cycle. For genotyping, genomic DNA was isolated by enzymatic digestion of tail clips using Direct-PCR Lysis Reagent (Viagen Biotech, Los Angeles, CA, USA). Genotypes were determined by performing PCR amplification of genomic DNA using allele-specific primers. The following primer sequences were used to yield genotype–specific amplicons of ~337 bp for the wild-type (WT) allele and ~475 bp for the KO allele: a WT-specific primer (5′-GCCTCTGACAGTGACCTCAGC-3′), a KO-specific primer (5′-CCTTCTATCGCCTTCTTGACG-3′), and a common primer (5′-GCTTCAGGTTCGCCACTCCCC-3′). All experiments were performed in accordance with National Institutes of Health (NIH) guidelines with approval from the Institutional Animal Care and Use Committee of the Louisiana State University Health Sciences Center-Shreveport.

### 2.2 Immunohistochemistry

Age- and sex-matched 6-month old WT (*Kcna1*$^{+/+}$; n=5: 3 males, 2 females) and KO mice (*Kcna1*$^{-/-}$; n=4: 2 males, 2 females) were used for immunohistochemical analysis. Older mice were selected for study to examine the long-term effects of chronic seizures, which begin at about 2 weeks old, thereby increasing the probability of accumulated brain pathology. Mice were transcardially perfused, first with phosphate buffered saline (PBS), then with 4% paraformaldehyde in PBS and lastly with 4% sucrose in PBS. After perfusion, the brains were removed and cryoprotected at 4°C for 3 days in a series of ascending sucrose solutions (10%, 20%, and 30% sucrose in PBS for one day each). Brains were then embedded in optimum cutting temperature medium (OCT) and frozen by placing at −80°C for 1 h. Brains were kept at −20°C for ~2 h immediately before coronal sectioning (10 μm) using a cryostat maintained at −20°C. Nuclear and antibody staining of serial sections was used to identify the following anatomical regions that fall within the Bregma coordinates as shown in the mouse brain atlas (Franklin and Paxinos, 2013): basolateral amygdala (Bregma −0.80 to −0.90 mm); hippocampus (Bregma −1.50 to −1.70 mm); parabrachial nucleus (PBP; Bregma −3.30 to −3.90 mm); retrotrapezoid nucleus (RTN), median raphae nucleus (MnR) and Kölliker-Fuse nucleus (KF; Bregma −4.80 to −5.15 mm); cerebellum (Bregma −5.40 to −8.00 mm); nucleus solitary tract (NTS; Bregma −6.50 to −7.00 mm); Bötzinger complex (Bregma −6.60 to −6.75 mm); nucleus ambiguus (NA; Bregma −6.60 to −7.30 mm); preBötzinger complex (Bregma Bregma −6.83 to −7.10 mm);

rostral ventral respiratory group (RVRG; Bregma −7.20 to −7.30 mm); and dorsal motor nucleus of vagus (10N) and hypoglossal nucleus (12N; Bregma −7.20 to −7.70 mm). After cutting, sections were blocked and permeabilized for 1 h in antibody vehicle (10% BSA, 0.3% Triton X-100 in PBS), followed by incubation in primary antibodies for 15–20 h at room temperature (~22 °C). Subsequently, sections were washed 3 times in vehicle and incubated for 1 h in secondary antibodies. Sections were then washed with vehicle once and PBS 3 times prior to staining with NucBlue Fixed Cell ReadyProbes reagent (Invitrogen; Life Technologies Co., Eugene, OR). Following a final wash in PBS, sections were slide-mounted using ProLong Glass Antifade Mountant without DAPI (Invitrogen; Life Technologies Co., Eugene, OR). Negative control experiments were performed by incubating sections with secondary antibodies in vehicle. Images were captured using an Olympus IX71 epifluorescence microscope with iVision as the acquisition software. Images were always acquired using the same optimized settings for each fluorophore. After acquisition, images were colorized using Fiji software, an image-processing package of ImageJ software (National Institutes of Health; Bethesda, MD, USA). Brightness and contrast were minimally adjusted to improve visualization of acquired images, but these settings were applied equally for each fluorophore for all images. Merged images were not further adjusted. Kv1.1 immunoreactivity was graded according to the approximate density of labeling and then assigned an incremental score of – (absent), + (low), ++ (moderate), or +++ (high). Quantification of GFAP and Iba1 immunoreactivity was performed using ImageJ to analyze images of the regions of interest from three pairs of age-matched WT and KO brains that had high-quality artifact-free sections for all brain regions under examination. After subtracting the background using a rolling ball radius of 50 pixels, binary images were generated and the percentage area occupied by positive immunoreactivity was measured for the entire region of interest in the field of view from three different nonconsecutive sections for a given brain.

### 2.3 Antibodies

The following primary antibodies and dilutions were used: mouse monoclonal anti-Kv1.1, 1:1000 (clone K20/78, Antibodies Incorporated, Davis, CA); rabbit polyclonal anti-neurokinin receptor 1 (NK1R), 1:5000 (S8305, Sigma-Aldrich, St. Louis, MO); rabbit polyclonal anti-Forkhead box protein P2 (FOXP2), 1:8000 (ab16046, Abcam, Cambridge, United Kingdom); mouse monoclonal anti-glial fibrillary acidic protein (GFAP) supernatant, 1:20 (clone N206A/8, Antibodies Incorporated, Davis, CA); rabbit polyclonal anti-ionized calcium binding adaptor molecule 1 (Iba1), 1:1000 (019–19741, Wako Chemicals, Richmond, VA). Secondary antibodies included Alexa Fluor 488 goat anti-mouse IgG1, 1:1000 (Invitrogen; Carlsbad, CA) and Alexa Fluor 594 goat anti-rabbit IgG, 1:1000 (Invitrogen; Carlsbad, CA).

### 2.4 Statistical analysis

Statistics were computed using Prism 9 software (GraphPad Software Inc., La Jolla, CA). Values are given as the mean ± standard error of the mean (SEM). For comparison of the percentage area occupied by immunoreactivity for the regions of interest between WT and KO animals, a nested two-tailed t-test was employed to account for the presence of repeated measures. Results were considered significant if $P < 0.05$.

# 3. RESULTS

## 3.1 Distribution of Kv1.1 immunoreactivity in wild-type (WT) mouse brain

Limbic system structures including the amygdala and hippocampus contain neurons that modulate respiration (Homma and Masaoka 2008; Dlouhy *et al.* 2015; Lhatoo *et al.* 2015; Nobis *et al.* 2019). Kv1.1 protein expression patterns have already been described in detail in hippocampus but not in the basolateral amygdala, which is known to be strongly activated by seizures in KO mice (Wang *et al.* 1994; Prüss *et al.* 2010; Gautier and Glasscock 2015). Moderate Kv1.1 immunoreactivity was detected in neuropil and some cell somata in basolateral amygdala (Figure 1). The density of Kv1.1 immunoreactivity in the amygdala and other brain regions examined is summarized in Table 1. Importantly, KO brains exhibited no significant Kv1.1 immunoreactivity in any brain regions, demonstrating the specificity of the Kv1.1 antibody staining.

The nucleus of the solitary tract (NTS) contains clusters of respiratory-modulated inspiratory neurons that act to coordinate respiratory reflex responses to afferent cardiorespiratory inputs from peripheral chemoreceptors, baroreceptors, and pulmonary stretch receptors (Zoccal *et al.* 2014). In NTS, neuropil and paired punctae consistent with juxtaparanodeal immunoreactivity of myelinated axons was observed, as previously observed for the vagus nerve (Glasscock *et al.* 2012; Glasscock *et al.* 2010; Wang *et al.* 1994) (Figure 2a). The localization of the axons is similar to the path of axons from the baroreceptive region of the NTS (Li *et al.* 2016). Thus, NTS, which is known for an important role in baroreception and respiration, exhibits significant Kv1.1 staining.

The dorsal motor nucleus of vagus (10N) is located along the floor of the fourth ventricle in the medulla and it is the nucleus for the vagus nerve, which provides parasympathetic efferents to the heart and other organs (Thompson *et al.* 2019). No Kv1.1 immunoreactivity was observed in 10N at lower magnification, but at higher magnification, low density Kv1.1 staining could be seen in some cell bodies (Figure 2b).

The hypoglossal nucleus (12N) is a cranial nerve motor nucleus which contains neurons that exhibit pre-inspiratory and inspiratory discharges that stabilize the upper airway prior to the commencement of airflow to the lungs (St. John *et al.* 2004). Reduction in eupneic ventilatory drive is observed when these discharges are uncoupled (St. John *et al.* 2004). Kv1.1 was highly expressed in the somata of these neurons and in associated fiber tracts (Figure 2c).

The ventral respiratory column (VRC) includes the Bötzinger nucleus, preBötzinger complex, and the rostral ventral respiratory group (RVRG) (Smith *et al.* 2009). The neurons of the VRC are involved in respiratory rhythm generation and their activity modulates the amplitude of respiratory motor output to spinal respiratory nerves (Alheid and McCrimmon 2008). The neighboring nucleus ambiguus (NA) houses preganglionic parasympathetic vagal neurons that innervate the heart and muscles of the soft palate, larynx, pharynx, adjusting ventilatory drive to respiratory muscle activity (Wijdicks 2017; Thompson *et al.* 2019). To aid in identification of the VRC and NA, Neurokinin–1 (NK1R) protein immunoreactivity was used as a marker since it specifically labels neurons of the Bötzinger nucleus, pre-

Bötzinger nucleus, RVRG, and NA (Forsberg *et al.* 2016; Wang *et al.* 2002). Moderate to high density somatic Kv1.1 staining was observed in cells of all VRC nuclei examined (Figure 3a–c). Kv1.1 labeling was also apparent in the neuropil of these regions, including prominent immunoreactivity consistent with juxtaparanodes of myelinated axons, similar to the staining pattern observed in the NTS (Figure 3a–d).

The dorsolateral and ventrolateral pons are critical mediators of respiratory responses in the Hering–Breuer mechanoreflex and carotid chemoreflex pathways (Song and Poon 2004). These structures are connected reciprocally with one another and with medullary nucleus tractus solitarius (NTS) and VRG. Pontomedullary signal processing plays an important role in respiratory rhythm modulation and control of breathing function (Song and Poon 2004). The pontine respiratory group encompasses the parabrachial and Kölliker–Fuse nuclei within the dorsolateral pons, consisting of several types of neurons that modulate respiration (Ezure and Tanaka 2006). Forkhead box protein 2 (FoxP2), a transcription factor, is a highly expressed protein in parabrachial and Kölliker fuse nuclei (Geerling *et al.* 2011). Thus, Foxp2 immunoreactivity was used as a marker to identify the pontine respiratory group. Moderate Kv1.1 staining was observed in the neuropil and fibers tracts passing through the parabrachial and Kölliker–Fuse nuclei (Figure 4a,b). Kv1.1 immunoreactivity was observed in somata and neuronal processes of both nuclei.

The retrotrapezoid nucleus (RTN), located in the rostral medulla, contains neurons that fire in response to increases in local $pCO_2$ and that innervate the regions of the brainstem that contain the respiratory pattern generator (Guyenet *et al.* 2012). Strong Kv1.1 staining was observed in neuropil and juxtaparanodal-like puncta of the RTN where Kv1.1 may play a role in chemoreception (Figure 5a).

Serotonergic neurons are important regulators of respiration and arousal and serotonergic signaling has been implicated in risk of sudden death in epilepsy (Richerson and Buchanan 2011; Hilaire *et al.* 2010). The raphe nuclei in the brainstem are the primary source of serotonergic neurons (Richerson and Buchanan 2011). High-density Kv1.1 immunoreactivity was observed in somata, neuropil, and juxtaparanodal-like puncta of the median raphae (Figure 5b).

### 3.2 Identification of astrogliosis

Seizures can injure the brain leading to reactive astrogliosis, which is defined by increased proliferation of astrocytes and characteristic changes in astrocytic morphology indicative of their reactive state, including hypertrophied cell bodies with abnormally long, extended processes. Thus, the presence of reactive astrocytes is an indicator of seizure-related brain damage that could lead to altered function (Sofroniew 2009; Patel *et al.* 2019). Using glial fibrillary acidic protein (GFAP) as a marker for astrocytes, we compared GFAP immunoreactivity in cardiorespiratory brain regions of adult WT (n=3) and KO (n=3) mouse brains to determine whether chronic seizures due to Kv1.1 deficiency induces astrogliosis. Overall, WT brains exhibited relatively sparse GFAP immunoreactivity in all regions examined with the highest density staining appearing in 10N and the Bötzinger complex (Figures 1–6). However, the GFAP-positive cells of the WT brains typically did not exhibit hypertrophic morphological changes indicative of reactive gliosis. In contrast, all KO brains

showed extensive GFAP immunoreactivity throughout all cardiorespiratory brain regions examined, including a significantly higher density of GFAP immunoreactivity and an abundance of cells with enlarged somata and long processes consistent with reactive gliosis (Figures 1–6). As summarized in Table 2, the density of GFAP immunoreactivity in KO brains relative to WT brains was highest in the basolateral amygdala and the parabrachial nucleus, which exhibited >6-fold increases. Most of the other nuclei examined exhibited 2-to 3-fold increases in GFAP immunoreactivity, except for the Bötzinger complex, 10N, and NTS, which exhibited more moderate but significant 1.2- to 1.7-fold increases.

### 3.3 Identification of microgliosis

Microglia are resident immune cells of the central nervous system constituting the first line of defense against pathogens or injury (Nimmerjahn *et al.* 2005). Similar to astrocytes, microglia proliferate and exhibit morphological changes in response to injury or infection leading to microgliosis (Fernández-Arjona *et al.* 2017; Torres-Platas *et al.* 2014). Using Iba1 (ionized calcium binding adaptor molecule-1) immunoreactivity as a specific marker of microglia, we compared microglial density between the brains of adult WT and KO mice to determine whether chronic seizures due to Kv1.1 deficiency induce microgliosis. In WT brains, Iba1-positive cells were present in all cardiorespiratory centers examined but they were relatively rare and low in abundance compared to KO mice (Figures 1–6). Conversely, in all KO mice, Iba-1 immunoreactivity appeared significantly more abundant than WT for all areas examined (Figures 1–6). As summarized in Table 2, the approximate densities of Iba1 immunoreactivity in KO brains (relative to WT) were highest in basolateral amygdala and the Bötzinger complex, which exhibited 23-fold and 14-fold increases, respectively. The median raphe, RTN, 12N, and NTS of KO brains also exhibited relatively large increases in Iba1 immunoreactivity ranging from 2- to 4-fold compared to WT. The other nuclei examined in KO brains showed more moderate but still significant 1- to 2-fold increases in Iba1 immunoreactivity.

## 4. DISCUSSION

This study provides the first description of Kv1.1 protein expression in the cardiorespiratory centers of normal mouse brain. Differential Kv1.1 immunoreactivity was detected in the main cardiorespiratory nuclei with the highest density of immunoreactivity observed in the NTS, hypoglossal nucleus, Botzinger nucleus, nucleus ambiguus, RTN, and median raphe nuclei. At the subcellular level, Kv1.1 immunoreactivity was evident in some cell bodies, but neuropil and axonal juxtaparanodal-like structures exhibited more prominent immunoreactivity. In *Kcna1*$^{-/-}$ mice, the presence of chronic seizures was associated with significantly greater GFAP and Iba1 immunoreactivity, consistent with astrogliosis and microgliosis, respectively, which could impair brain function. Thus, the presence of Kv1.1 immunoreactivity in cardiorespiratory brain centers suggests that Kv1.1-containing channels could contribute to intrinsic control of breathing and that absence of Kv1.1 in *Kcna1*$^{-/-}$ mice could result in seizure-induced brain damage in the neurocircuits for respiratory function.

Any of the cardiorespiratory brain regions examined in this work could potentially contribute to the basal and seizure-associated cardiorespiratory phenotypes in *Kcna1*$^{-/-}$

mice, but one structure that is of special interest is the amygdala. Although not part of the canonical brainstem cardiorespiratory circuitry, limbic structures including the amygdala can exert powerful influence over respiration, especially during seizures (Dlouhy *et al.* 2015; Nobis *et al.* 2019; Lacuey *et al.* 2017; Applegate *et al.* 1983; Kaada and Jasper 1952; Harper *et al.* 1984). In patients, the onset of apneas is strongly correlated with the spread of seizures to the amygdala or with electrical stimulation of the amygdala (Dlouhy *et al.* 2015; Nobis *et al.* 2019; Lacuey *et al.* 2017). Stimulation of the hippocampus, another limbic structure which strongly expresses Kv1.1, can also evoke apneas in epilepsy patients (Lacuey *et al.* 2017; Wang *et al.* 1994). In *Kcna1*$^{-/-}$ mice, Fos immunostaining reveals that spontaneous seizures activate hippocampal and amygdalar circuits, which could contribute to the occurrence of ictal respiratory dysfunction in these animals (Gautier and Glasscock 2015; Dhaibar *et al.* 2019). The ability of the amygdala to influence respiration is likely due to its extensive projections to brainstem respiratory neurons, including connections with the respiratory rhythm generating pre-Botzinger complex (Yang *et al.* 2020; Price and Amaral 1981; Hopkins 1975). Thus, the absence of Kv1.1 could lead to neuronal excitability defects in the amygdala that alter respiration, and excessive activity due to seizures in *Kcna1*$^{-/-}$ mice could evoke downstream breathing dysfunction.

The brains of *Kcna1*$^{-/-}$ mice exhibited extensive activation of astrocytes and microglia throughout cardiorespiratory centers, indicative of brain injury sustained by the occurrence of repeated spontaneous seizures. Glial activation, or reactive gliosis, occurs in response to central nervous system insults such as seizures, and it is considered an integral part of epilepsy histopathology (Patel *et al.* 2019). The hallmarks of reactive gliosis include hypertrophy of cell bodies and processes and upregulated expression of GFAP and Iba1 in astrocytes and microglia, respectively (Patel *et al.* 2019). Reactive astrocytes increase neuronal hyperexcitability because they are unable to clear extracellular $K^+$ and glutamate, resulting in reduced GABAergic inhibition of neurons (Patel *et al.* 2019; Robel and Sontheimer 2016). Reactive microglia also release proinflammatory cytokines which can lead to neuronal hyperexcitability and neurodegeneration that exacerbates epilepsy (Victor and Tsirka 2020; Hiragi *et al.* 2018). Previous studies have found varying degrees of astrogliosis in the hippocampus and hypothalamus of *Kcna1*$^{-/-}$ mice depending upon seizure severity, duration, and frequency (Wenzel *et al.* 2007; Roundtree *et al.* 2016). In addition, extensive seizure-related neurodegeneration and cell loss have been observed in the hippocampus and amygdala of *Kcna1*$^{-/-}$ mice, as well as in neocortex, piriform cortex and thalamus (Wenzel *et al.* 2007). Here, our study reveals that the extent of gliosis in *Kcna1*$^{-/-}$ mice extends beyond forebrain and limbic structures to include brainstem cardiorespiratory centers. Increased gliosis in brainstem respiratory control centers has also been observed in victims of sudden infant death syndrome (SIDS) (Takashima *et al.* 1978; Bruce and Becker 1991). Thus, the gliosis in the cardiorespiratory neurocircuits of *Kcna1*$^{-/-}$ mice observed here suggests that these brain networks are recruited during spontaneous seizures leading to pathological changes that could alter neuronal excitability and impair cardiorespiratory function.

This study provides an initial survey of Kv1.1 expression and gliosis in cardiorespiratory brain centers as a starting point for more detailed studies. However, the study contains several limitations that can guide these studies. First, Kv1.1 immunoreactivity was strongest

for neuropil and fiber tracts rather than cell bodies, hindering the ability to unambiguously assign Kv1.1 expression to particular neuronal populations. For example, it is possible that the Kv1.1 immunoreactivity could be associated with axons or terminals that belong to different nearby structures that are synapsing on the neurons of interest. Future studies with tracer molecules and higher-resolution imaging could help distinguish the precise neuronal origin of Kv1.1-immunoreactive axons. More in-depth molecular characterization will also be required to determine the functional nature of the Kv1.1 immunoreactivity identified in this study (e.g., excitatory vs. inhibitory neurons; axonal vs. dendritic vs. synaptic terminal). Similarly, reactive astrocytes and microglia also exhibit distinct functional types (such as A1 vs. A2 for astrocytes or M1 vs. M2 for microglia) that are distinguishable by their specific molecular expression changes (Cherry *et al.* 2014; Li *et al.* 2019); discrimination of subtype-specific gliosis was beyond the scope of this study. Finally, cellular electrophysiological approaches will be required to determine the precise functional roles of Kv1.1 in the neural circuitry of the various cardiorespiratory brain regions.

In summary, this work describes widespread differential Kv1.1 expression in brain cardiorespiratory centers, which strengthens the hypothesis that Kv1.1 plays an important role in the intrinsic control of respiration. In *Kcna1*$^{-/-}$ mice, the presence of extensive gliosis in cardiorespiratory networks suggests the absence of Kv1.1 is associated with, if not causative for, seizure-related remodeling and damage. Thus, *Kcna1* gene deletion may lead to respiratory dysfunction either directly by inducing hyperexcitability in Kv1.1-deficient respiratory neurons, or indirectly by causing accumulation of seizure-related damage in respiratory brain networks.

## ACKNOWLEDGEMENTS

**Funding:**

The study was supported by grants from the National Institutes of Health (NS100954 and NS099188 to EG) and by an Ike Muslow pre-doctoral fellowship from the Louisiana State University Health Sciences Center-Shreveport to H.D.

## Data availability:

The data that support the findings of this study are available from the corresponding author upon reasonable request.

## REFERENCES

Alheid GF, McCrimmon DR (2008) The chemical neuroanatomy of breathing. Respir. Physiol. Neurobiol. 164, 3–11. [PubMed: 18706532]

Applegate CD, Kapp BS, Underwood MD, McNall CL (1983) Autonomic and somatomotor effects of amygdala central N. stimulation in awake rabbits. Physiol. Behav. 31, 353–360. [PubMed: 6635005]

Bruce K, Becker LE (1991) Quantitation of Medullary Astrogliosis in Sudden Infant Death Syndrome. Pediatr. Neurosurg. 17, 74–79. [PubMed: 1815732]

Cherry JD, Olschowka JA, O'Banion MK (2014) Neuroinflammation and M2 microglia: the good, the bad, and the inflamed. J. Neuroinflammation 11, 98. [PubMed: 24889886]

Devinsky O, Vezzani A, Najjar S, De Lanerolle NC, Rogawski MA (2013) Glia and epilepsy: excitability and inflammation. Trends Neurosci. 36, 174–184. [PubMed: 23298414]

Dhaibar H, Gautier NM, Chernyshev OY, Dominic P, Glasscock E (2019) Cardiorespiratory profiling reveals primary breathing dysfunction in Kcna1-null mice: Implications for sudden unexpected death in epilepsy. Neurobiol. Dis. 127, 502–511. [PubMed: 30974168]

Dlouhy BJ, Gehlbach BK, Kreple CJ, Kawasaki H, Oya H, Buzza C, Granner MA, et al. (2015) Breathing Inhibited When Seizures Spread to the Amygdala and upon Amygdala Stimulation. J. Neurosci. 35, 10281–10289. [PubMed: 26180203]

Ezure K, Tanaka I (2006) Distribution and medullary projection of respiratory neurons in the dorsolateral pons of the rat. Neuroscience 141, 1011–1023. [PubMed: 16725272]

Feng H-J, Faingold CL (2017) Abnormalities of serotonergic neurotransmission in animal models of SUDEP. Epilepsy Behav. 71, 174–180. [PubMed: 26272185]

Fernández-Arjona M del M, Grondona JM, Granados-Durán P, Fernández-Llebrez P, López-Ávalos MD (2017) Microglia Morphological Categorization in a Rat Model of Neuroinflammation by Hierarchical Cluster and Principal Components Analysis. Front. Cell. Neurosci. 11.

Forsberg D, Horn Z, Tserga E, Smedler E, Silberberg G, Shvarev Y, Kaila K, Uhlén P, Herlenius E (2016) CO2-evoked release of PGE2 modulates sighs and inspiration as demonstrated in brainstem organotypic culture. eLife 5, e14170. [PubMed: 27377173]

Gautier NM, Glasscock E (2015) Spontaneous seizures in Kcna1-null mice lacking voltage-gated Kv1.1 channels activate Fos expression in select limbic circuits. J. Neurochem. 135, 157–164. [PubMed: 26112121]

Geerling JC, Stein MK, Miller RL, Shin J-W, Gray PA, Loewy AD (2011) FoxP2 expression defines dorsolateral pontine neurons activated by sodium deprivation. Brain Res. 1375, 19–27. [PubMed: 21108936]

Glasscock E (2019) Kv1.1 channel subunits in the control of neurocardiac function. Channels Austin Tex 13, 299–307. [PubMed: 31250689]

Glasscock E, Qian J, Kole MJ, Noebels JL (2012) Transcompartmental reversal of single fibre hyperexcitability in juxtaparanodal Kv1.1-deficient vagus nerve axons by activation of nodal KCNQ channels. J. Physiol. 590, 3913–3926. [PubMed: 22641786]

Glasscock E, Yoo JW, Chen TT, Klassen TL, Noebels JL (2010) Kv1.1 potassium channel deficiency reveals brain-driven cardiac dysfunction as a candidate mechanism for sudden unexplained death in epilepsy. J. Neurosci. 30, 5167–5175. [PubMed: 20392939]

Grass D, Pawlowski PG, Hirrlinger J, Papadopoulos N, Richter DW, Kirchhoff F, Hülsmann S (2004) Diversity of functional astroglial properties in the respiratory network. J. Neurosci. 24, 1358–1365. [PubMed: 14960607]

Guyenet PG, Stornetta RL, Abbott SBG, Depuy SD, Kanbar R (2012) The Retrotrapezoid Nucleus and Breathing. Adv. Exp. Med. Biol. 758, 115–122. [PubMed: 23080151]

Harper RM, Frysinger RC, Trelease RB, Marks JD (1984) State-dependent alteration of respiratory cycle timing by stimulation of the central nucleus of the amygdala. Brain Res. 306, 1–8. [PubMed: 6466967]

Hilaire G, Voituron N, Menuet C, Ichiyama RM, Subramanian HH, Dutschmann M (2010) The role of serotonin in respiratory function and dysfunction. Respir. Physiol. Neurobiol. 174, 76–88. [PubMed: 20801236]

Hiragi T, Ikegaya Y, Koyama R (2018) Microglia after Seizures and in Epilepsy. Cells 7.

Homma I, Masaoka Y (2008) Breathing rhythms and emotions. Exp. Physiol. 93, 1011–1021. [PubMed: 18487316]

Hopkins DA (1975) Amygdalotegmental projections in the rat, cat and rhesus monkey. Neurosci. Lett. 1, 263–270. [PubMed: 19604788]

Kaada BR, Jasper H (1952) Respiratory responses to stimulation of temporal pole, insula, and hippocampal and limbic gyri in man. AMA Arch. Neurol. Psychiatry 68, 609–619. [PubMed: 12984874]

Kennedy JD, Seyal M (2015) Respiratory pathophysiology with seizures and implications for sudden unexpected death in epilepsy. J. Clin. Neurophysiol. Off. Publ. Am. Electroencephalogr. Soc. 32, 10–13.

Kim Y, Bravo E, Thirnbeck CK, Smith-Mellecker LA, Kim SH, Gehlbach BK, Laux LC, Zhou X, Nordli DR, Richerson GB (2018) Severe peri-ictal respiratory dysfunction is common in Dravet syndrome. J. Clin. Invest. 128, 1141–1153. [PubMed: 29329111]

Kruse SW, Dayton KG, Purnell BS, Rosner JI, Buchanan GF (2019) Effect of monoamine reuptake inhibition and α1 blockade on respiratory arrest and death following electroshock-induced seizures in mice. Epilepsia 60, 495–507. [PubMed: 30723893]

Lacuey N, Zonjy B, Londono L, Lhatoo SD (2017) Amygdala and hippocampus are symptomatogenic zones for central apneic seizures. Neurology 88, 701–705. [PubMed: 28087822]

Lhatoo S, Noebels J, Whittemore V, NINDS Center for SUDEP Research (2015) Sudden unexpected death in epilepsy: Identifying risk and preventing mortality. Epilepsia 56, 1700–1706. [PubMed: 26494436]

Li C, Fitzgerald MEC, Del Mar N, Reiner A (2016) Stimulation of Baroresponsive Parts of the Nucleus of the Solitary Tract Produces Nitric Oxide-mediated Choroidal Vasodilation in Rat Eye. Front. Neuroanat. 10.

Li K, Li J, Zheng J, Qin S (2019) Reactive Astrocytes in Neurodegenerative Diseases. Aging Dis. 10, 664–675. [PubMed: 31165009]

Nimmerjahn A, Kirchhoff F, Helmchen F (2005) Resting Microglial Cells Are Highly Dynamic Surveillants of Brain Parenchyma in Vivo. Science 308, 1314–1318. [PubMed: 15831717]

Nobis WP, González Otárula KA, Templer JW, Gerard EE, VanHaerents S, Lane G, Zhou G, Rosenow JM, Zelano C, Schuele S (2019) The effect of seizure spread to the amygdala on respiration and onset of ictal central apnea. J. Neurosurg, 1–11.

Patel DC, Tewari BP, Chaunsali L, Sontheimer H (2019) Neuron-glia interactions in the pathophysiology of epilepsy. Nat. Rev. Neurosci. 20, 282–297. [PubMed: 30792501]

Price JL, Amaral DG (1981) An autoradiographic study of the projections of the central nucleus of the monkey amygdala. J. Neurosci. Off. J. Soc. Neurosci. 1, 1242–1259.

Prüss H, Grosse G, Brunk I, Veh RW, Ahnert-Hilger G (2010) Age-dependent axonal expression of potassium channel proteins during development in mouse hippocampus. Histochem. Cell Biol. 133, 301–312. [PubMed: 20012645]

Richerson GB, Buchanan GF (2011) The serotonin axis: Shared mechanisms in seizures, depression, and SUDEP. Epilepsia 52 Suppl 1, 28–38.

Robel S, Sontheimer H (2016) Glia as drivers of abnormal neuronal activity. Nat. Neurosci. 19, 28–33. [PubMed: 26713746]

Roundtree HM, Simeone TA, Johnson C, Matthews SA, Samson KK, Simeone KA (2016) Orexin Receptor Antagonism Improves Sleep and Reduces Seizures in Kcna1-null Mice. Sleep 39, 357–368. [PubMed: 26446112]

Ryvlin P, Nashef L, Lhatoo SD, Bateman LM, Bird J, Bleasel A, Boon P, et al. (2013) Incidence and mechanisms of cardiorespiratory arrests in epilepsy monitoring units (MORTEMUS): a retrospective study. Lancet Neurol. 12, 966–977. [PubMed: 24012372]

Sheikhbahaei S, Turovsky EA, Hosford PS, Hadjihambi A, Theparambil SM, Liu B, Marina N, et al. (2018) Astrocytes modulate brainstem respiratory rhythmgenerating circuits and determine exercise capacity. Nat. Commun. 9, 370. [PubMed: 29371650]

Simeone KA, Hallgren J, Bockman CS, Aggarwal A, Kansal V, Netzel L, Iyer SH, et al. (2018) Respiratory dysfunction progresses with age in Kcna1-null mice, a model of sudden unexpected death in epilepsy. Epilepsia 59, 345–357. [PubMed: 29327348]

Smart SL, Lopantsev V, Zhang CL, Robbins CA, Wang H, Chiu SY, Schwartzkroin PA, Messing A, Tempel BL (1998) Deletion of the KV1.1 Potassium Channel Causes Epilepsy in Mice. Neuron 20, 809–819. [PubMed: 9581771]

Smith JC, Abdala APL, Rybak IA, Paton JFR (2009) Structural and functional architecture of respiratory networks in the mammalian brainstem. Philos. Trans. R. Soc. Lond. B. Biol. Sci. 364, 2577–2587. [PubMed: 19651658]

Sofroniew MV (2009) Molecular dissection of reactive astrogliosis and glial scar formation. Trends Neurosci. 32, 638–647. [PubMed: 19782411]

Song G, Poon C-S (2004) Functional and structural models of pontine modulation of mechanoreceptor and chemoreceptor reflexes. Respir. Physiol. Neurobiol. 143, 281–292. [PubMed: 15519561]

St. John WM, Paton JFR, Leiter JC (2004) Uncoupling of rhythmic hypoglossal from phrenic activity in the rat. Exp. Physiol. 89, 727–737. [PubMed: 15364882]

Takashima S, Armstrong D, Becker L, Bryan C (1978) Cerebral hypoperfusion in the sudden infant death syndrome? brainstem gliosis and vasculature. Ann. Neurol. 4, 257–262. [PubMed: 718138]

Thompson N, Mastitskaya S, Holder D (2019) Avoiding off-target effects in electrical stimulation of the cervical vagus nerve: Neuroanatomical tracing techniques to study fascicular anatomy of the vagus nerve. J. Neurosci. Methods 325, 108325. [PubMed: 31260728]

Torres-Platas SG, Comeau S, Rachalski A, Bo GD, Cruceanu C, Turecki G, Giros B, Mechawar N (2014) Morphometric characterization of microglial phenotypes in human cerebral cortex. J. Neuroinflammation 11, 12. [PubMed: 24447857]

Trosclair K, Dhaibar HA, Gautier NM, Mishra V, Glasscock E (2020) Neuron-specific Kv1.1 deficiency is sufficient to cause epilepsy, premature death, and cardiorespiratory dysregulation. Neurobiol. Dis. 137, 104759. [PubMed: 31978607]

Victor TR, Tsirka SE (2020) Microglial contributions to aberrant neurogenesis and pathophysiology of epilepsy. Neuroimmunol. Neuroinflammation 7, 234–247.

Wang H, Germanson TP, Guyenet PG (2002) Depressor and tachypneic responses to chemical stimulation of the ventral respiratory group are reduced by ablation of neurokinin-1 receptor-expressing neurons. J. Neurosci. 22, 3755–3764. [PubMed: 11978851]

Wang H, Kunkel DD, Schwartzkroin PA, Tempel BL (1994) Localization of Kv1.1 and Kv1.2, two K channel proteins, to synaptic terminals, somata, and dendrites in the mouse brain. J. Neurosci. 14, 4588–4599. [PubMed: 8046438]

Wenker IC, Teran FA, Wengert ER, Wagley PK, Panchal PS, Blizzard EA, Saraf P, et al. (2021) Postictal Death Is Associated with Tonic Phase Apnea in a Mouse Model of Sudden Unexpected Death in Epilepsy. Ann. Neurol.

Wenzel HJ, Vacher H, Clark E, Trimmer JS, Lee AL, Sapolsky RM, Tempel BL, Schwartzkroin PA (2007) Structural consequences of Kcna1 gene deletion and transfer in the mouse hippocampus. Epilepsia 48, 2023–2046. [PubMed: 17651419]

Wijdicks EFM (2017) The neurology of acutely failing respiratory mechanics. Ann. Neurol. 81, 485–494. [PubMed: 28253561]

Yang CF, Kim EJ, Callaway EM, Feldman JL (2020) Monosynaptic Projections to Excitatory and Inhibitory preBötzinger Complex Neurons. Front. Neuroanat. 14, 58. [PubMed: 33013329]

Zoccal DB, Furuya WI, Bassi M, Colombari DSA, Colombari E (2014) The nucleus of the solitary tract and the coordination of respiratory and sympathetic activities. Front. Physiol. 5.

## Highlights

- Kv1.1 knockout (KO) mice have lethal seizures involving cardiorespiratory dysfunction
- Wild-type mice exhibited Kv1.1 immunoreactivity in cardiorespiratory brain centers
- KO mice showed extensive GFAP and Iba1 immunoreactivity in brainstem indicative of gliosis
- Kv1.1 deficiency may impair breathing intrinsically or by seizure-induced injury

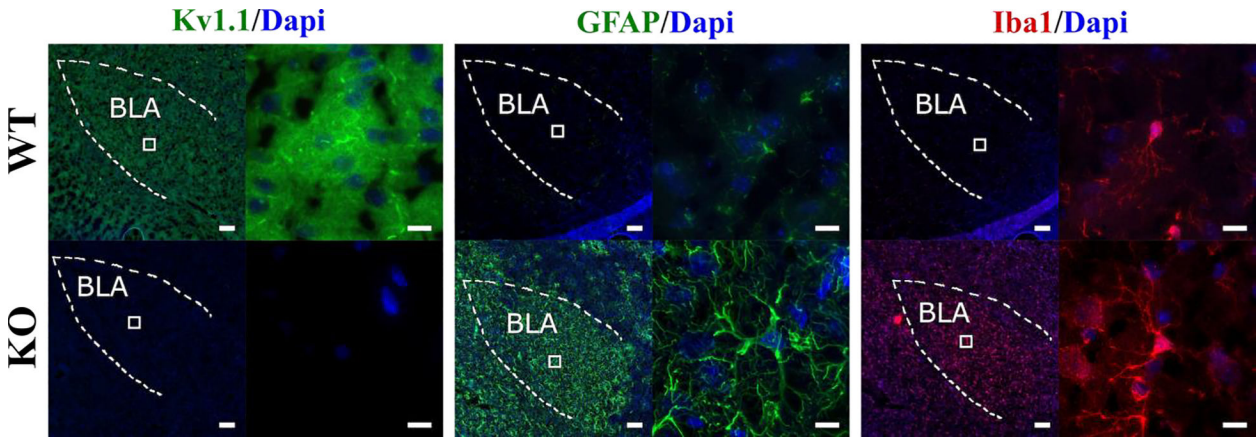


**Figure 1.**

Kv1.1, GFAP, and Iba1 immunoreactivity in basolateral amygdala (BLA) of wild–type (WT) and *Kcna1*$^{-/-}$ (KO) mice. In each figure, the left panel shows a lower magnification image (scale bar = 100 μm) and the right panel shows a higher magnification image (scale bar = 10 μm) of the boxed region. The dotted lines represent the boundary of the brain region. DAPI staining was used to label the nuclei of cells.

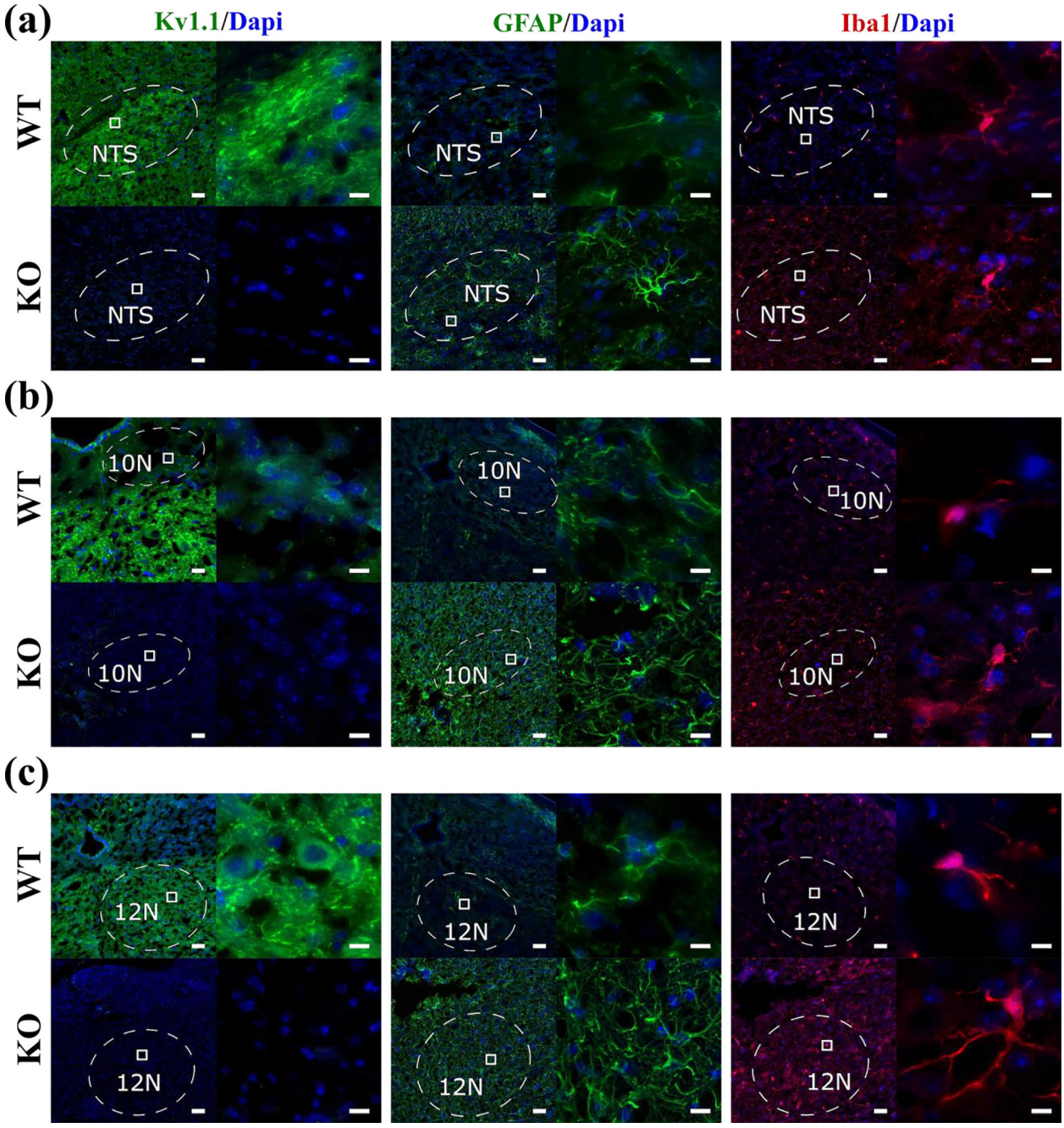


**Figure 2.**

Kv1.1, GFAP, and Iba1 immunoreactivity in the dorsal respiratory group and nearby cardiorespitory nuclei in wild–type (WT) and *Kcna1*$^{-/-}$ (KO) mice. The structures shown include the (a) nucleus of the solitary tract (NTS), (b) dorsal motor nucleus of vagus (10N), and (c) hypoglossal nucleus (12N). For each condition, the left panel shows a lower magnification image (scale bar = 100 μm) and the right panel shows a higher magnification image (scale bar = 10 μm) corresponding to the boxed region in the left panel. The dotted lines represent the boundary of the respective brain region being examined. DAPI staining was used to label the nuclei of cells.

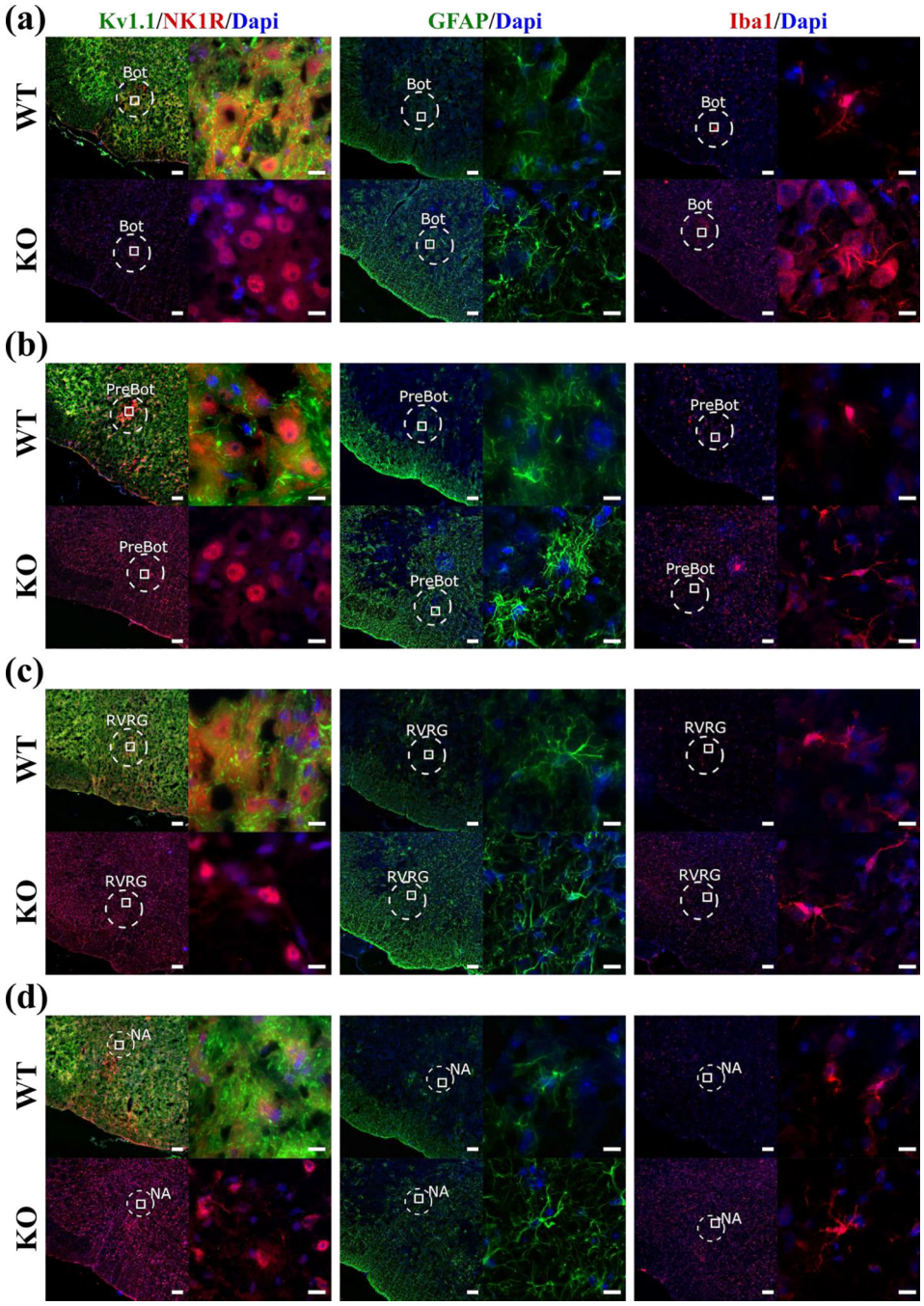


**Figure 3.**

Kv1.1, GFAP, and Iba1 immunoreactivity in the ventral respiratory column and nucleus ambiguus (NA) of wild–type (WT) and *Kcna1*$^{-/-}$ (KO) mice. The structures shown include the (a) Bötzinger complex (Bot), (b) preBötzinger complex (preBot), (c) rostral ventral respiratory group (RVRG), and (d) NA. For each condition, the left panel shows a lower magnification image (scale bar = 100 μm) and the right panel shows a higher magnification image (scale bar = 10 μm) corresponding to the boxed region in the left panel. The dotted lines represent the boundary of the respective brain region being examined. DAPI staining

was used to label the nuclei of cells. NK1R immunoreactivity, which is present in the neurons of the ventral respiratory column, was used to aid positive identification of the cells of the various nuclei.

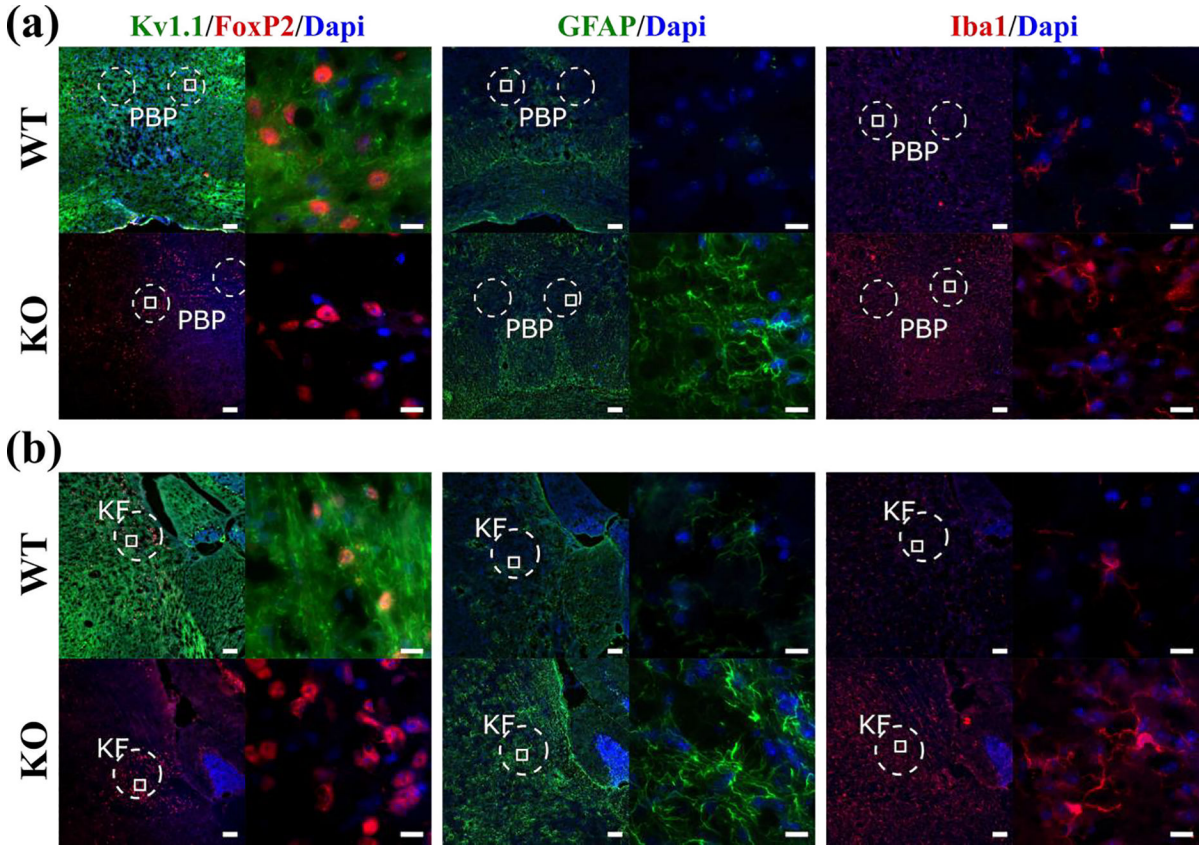


**Figure 4.**

Kv1.1, GFAP, and Iba1 immunoreactivity in the pontine respiratory group of wild–type (WT) and *Kcna1*$^{-/-}$ (KO) mice. The structures shown include the in (a) parabrachial nucleus (PBP) and (b) Kölliker fuse nucleus (KF). For each condition, the left panel shows a lower magnification image (scale bar = 100 μm) and the right panel shows a higher magnification image (scale bar = 10 μm) corresponding to the boxed region in the left panel. The dotted lines represent the boundary of the respective brain region being examined. DAPI staining was used to label the nuclei of cells. FoxP2 immunoreactivity, which is present in the neurons of PBP and KF, was used to aid positive identification of these nuclei.

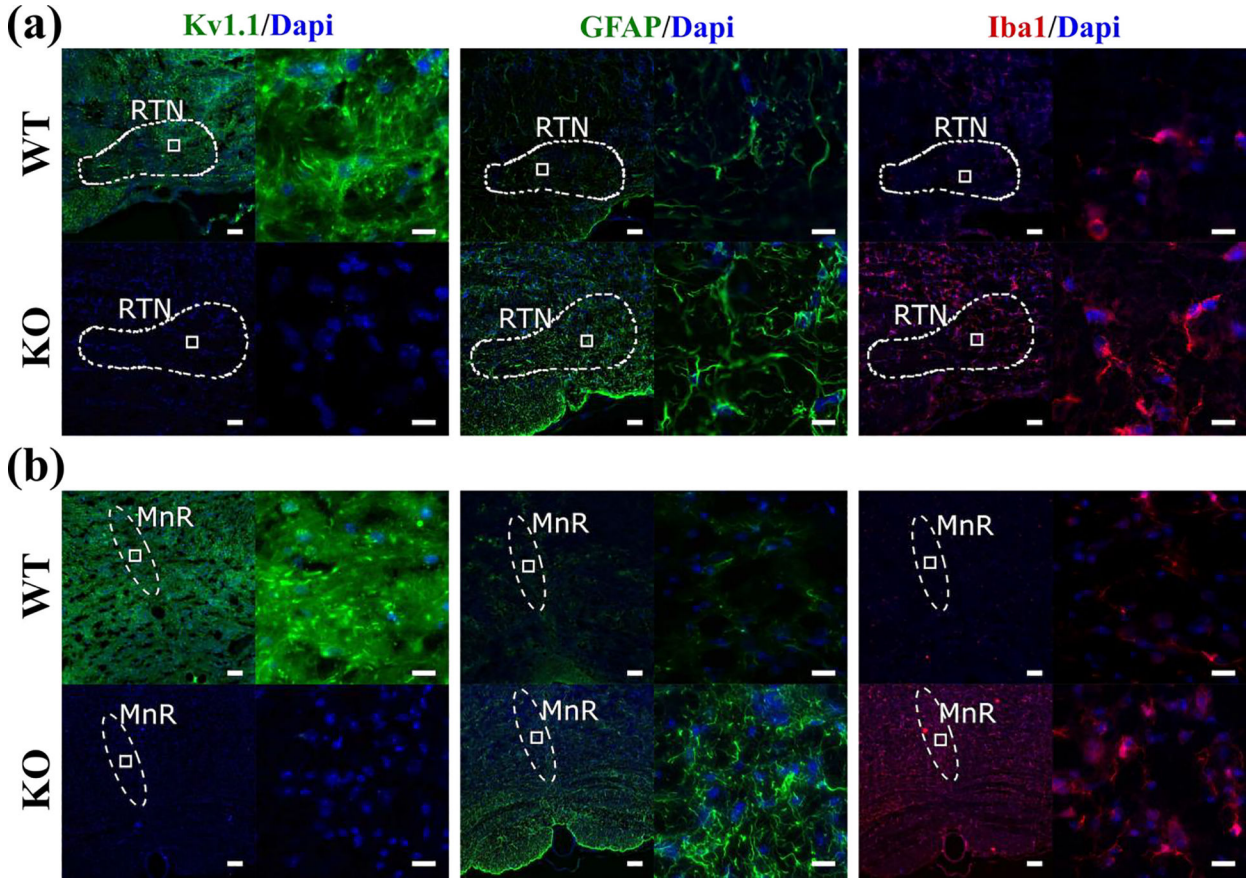


**Figure 5.**

Kv1.1, GFAP, and Iba1 immunoreactivity in chemosensory brain regions in wild–type (WT) and *Kcna1*$^{-/-}$ (KO) mice. The structures shown include the (a) retrotrapezoid nucleus (RTN) and (b) median raphe nucleus (MnR). For each condition, the left panel shows a lower magnification image (scale bar = 100 μm) and the right panel shows a higher magnification image (scale bar = 10 μm) corresponding to the boxed region in the left panel. The dotted lines represent the boundary of the respective brain region being examined. DAPI staining was used to label the nuclei of cells.

**Table 1.**

Summary of Kv1.1 immunoreactivity density in respiratory brain regions in WT mice.

| Structural group | Nucleus | Kv1.1 |
|---|---|---|
| Limbic system | basolateral amygdala | ++ |
| Dorsal respiratory group (and nearby nuclei) | nucleus of the solitary tract | +++ |
| | dorsal motor nucleus of vagus | + |
| | hypoglossal nucleus | +++ |
| Ventral respiratory column (and nearby nuclei) | Bötzinger complex | +++ |
| | preBötzinger complex | ++ |
| | rostral ventral respiratory group | ++ |
| | nucleus ambiguus | +++ |
| Pontine respiratory group | parabrachial nucleus | ++ |
| | Kölliker fuse nucleus | ++ |
| Chemosensory centers | retrotrapezoid nucleus | +++ |
| | median raphe | +++ |

The plus signs (+) indicate relative immunoreactivity density with (+) being the lowest (but still present) and (+++) being the highest.

**Table 2.**

Summary of GFAP and Iba1 immunoreactivity density in respiratory brain regions in age-matched WT and KO mice (n=3/genotype).

| | | GFAP (% area of positive immunoreactivity) | | | Iba1 (% area of positive immunoreactivity) | | |
|---|---|---|---|---|---|---|---|
| **Structural group** | **Nucleus** | **WT** | **KO** | **P-value** | **WT** | **KO** | **P-value** |
| Limbic system | basolateral amygdala | 2.1±0.11 | 13.1±0.17 | <0.0001 | 0.5±0.01 | 11.0±0.06 | <0.0001 |
| Dorsal respiratory group (and nearby nuclei) | nucleus of the solitary tract | 7.9±0.15 | 10.0±0.09 | 0.0149 | 6.1±0.03 | 13.0±0.08 | 0.0002 |
| | dorsal motor nucleus of vagus | 9.9±0.07 | 13.6±0.09 | 0.0053 | 5.9±0.03 | 9.5±0.28 | 0.0008 |
| | hypoglossal nucleus | 5.6±0.19 | 11.8±0.17 | <0.0001 | 5.5±0.03 | 15.6±0.23 | <0.0001 |
| Ventral respiratory column (and nearby nuclei) | Bötzinger complex | 9.9±0.01 | 16.4±0.07 | 0.0007 | 1.5±0.10 | 20.4±0.07 | <0.0001 |
| | preBötzinge r complex | 6.3±0.12 | 15.4±0.29 | 0.0006 | 10.1±0.24 | 16.5±0.16 | 0.0021 |
| | rostral ventral respiratory group | 5.4±0.19 | 14.2±0.18 | 0.0001 | 13.6±0.10 | 20.0±0.29 | 0.0022 |
| | nucleus ambiguus | 2.7±0.02 | 9.2±0.01 | <0.0001 | 7.4±0.32 | 13.2±0.16 | <0.0001 |
| Pontine respiratory group | parabrachial nucleus | 1.7±0.01 | 15.2±0.48 | <0.0001 | 11.4±0.13 | 17.0±0.29 | 0.0021 |
| | Kölliker fuse nucleus | 3.7±0.11 | 9.3±0.01 | 0.0007 | 5.4±0.27 | 10.1±0.07 | 0.0025 |
| Chemosensory centers | retrotrapezoid nucleus | 6.9±0.10 | 14.4±0.25 | 0.0021 | 5.8±0.19 | 14.1±0.52 | <0.0001 |
| | median raphe | 3.0±0.37 | 8.7±0.04 | <0.0001 | 3.4±0.53 | 15.9±0.21 | 0.0002 |

Values given as the mean ± SEM. P-values calculated using nested two-tailed t-tests.